



University of HUDDERSFIELD

University of Huddersfield Repository

Pesce, Giovanni L., Fletcher, Ian W., Grant, James, Molinari, Marco, Parker, Stephen C. and Ball, Richard J.

Carbonation of Hydrous Materials at the Molecular Level: A Time of Flight-Secondary Ion Mass Spectrometry, Raman and Density Functional Theory Study

Original Citation

Pesce, Giovanni L., Fletcher, Ian W., Grant, James, Molinari, Marco, Parker, Stephen C. and Ball, Richard J. (2017) Carbonation of Hydrous Materials at the Molecular Level: A Time of Flight-Secondary Ion Mass Spectrometry, Raman and Density Functional Theory Study. *Crystal Growth and Design*, 17 (3). pp. 1036-1044. ISSN 1528-7505

This version is available at <http://eprints.hud.ac.uk/id/eprint/33340/>

The University Repository is a digital collection of the research output of the University, available on Open Access. Copyright and Moral Rights for the items on this site are retained by the individual author and/or other copyright owners. Users may access full items free of charge; copies of full text items generally can be reproduced, displayed or performed and given to third parties in any format or medium for personal research or study, educational or not-for-profit purposes without prior permission or charge, provided:

- The authors, title and full bibliographic details is credited in any copy;
- A hyperlink and/or URL is included for the original metadata page; and
- The content is not changed in any way.

For more information, including our policy and submission procedure, please contact the Repository Team at: E.mailbox@hud.ac.uk.

<http://eprints.hud.ac.uk/>

Carbonation of Hydrous Materials at the Molecular Level: a ToF-SIMS, Raman and DFT study

Giovanni L. Pesce¹, Ian Fletcher², James Grant³, Marco Molinari^{3,4}, Stephen C. Parker^{3,},*

Richard J. Ball¹

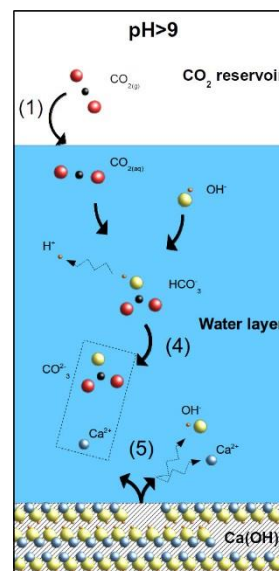
¹ University of Bath, Department of Arch. and Civil Engineering, Bath, BA2 7AY, UK

² Intertek Wilton Laboratory, The Wilton Centre, Redcar, TS10 4RF, UK

³ University of Bath, Department of Chemistry, Bath, BA2 7AY, UK

⁴Department of Chemistry, University of Huddersfield, Queensgate, Huddersfield, HD1 3DH, UK

Carbonation of hydrous minerals such as calcium hydroxide ($\text{Ca}(\text{OH})_2$), is an important process in environmental and industrial applications for the construction industry, geological disposal repositories for nuclear waste, and green technologies for carbon capture. Although the role of ions during the carbonation mechanism of $\text{Ca}(\text{OH})_2$ is still unclear, we identified the exchange of ions during the dissolution-and-precipitation process, by determining the change in isotopic composition of carbonation products using Time-of-Flight Secondary Ion Mass Spectrometry. Our samples of pure $\text{Ca}({}^{18}\text{OH})_2$ carbonated in air were characterized using Scanning Electron Microscopy and Raman spectroscopy, aided by Density Functional Theory calculations. Our results show that the carbonation process at high pH is a two-stage mechanism. The first stage occurs in a short time after $\text{Ca}({}^{18}\text{OH})_2$ is exposed to air and involved the dissolution of surface Ca ions and hydroxyl ${}^{18}\text{OH}$ groups, which reacts directly with dissolved CO_2 , leading to 1/3 of ${}^{18}\text{O}$ in the oxygen content of carbonate phases. The second stage occurs within 24h of exposure allowing a rebalance of the oxygen isotopic composition of the carbonate phases with higher content of ${}^{16}\text{O}$.



Prof. Steve Parker, Department of Chemistry, University of Bath, BA2 7AY, Bath United Kingdom, E: S.C.Parker@bath.ac.uk

Carbonation of Hydrous Materials at the Molecular Level: a ToF-SIMS, Raman and DFT study

*Giovanni L. Pesce^{1, i}, Ian Fletcher^{2, ii}, James Grant³, Marco Molinari^{3, 4}, Stephen C. Parker^{3, *},
Richard J. Ball¹*

¹ University of Bath, Department of Arch. and Civil Engineering, Bath, BA2 7AY, UK

² Intertek Wilton Laboratory, The Wilton Centre, Redcar, TS10 4RF, UK

³ University of Bath, Department of Chemistry, Bath, BA2 7AY, UK

⁴ Department of Chemistry, University of Huddersfield, Queensgate, Huddersfield, HD1
3DH, UK

* Corresponding authors: Stephen C. Parker, S.C.Parker@bath.ac.uk, phone: +44 (0)1225
386505

ⁱ Currently at Northumbria University, Department of Architecture and Built Environment,
Newcastle upon Tyne, NE1 8ST, UK

ⁱⁱ Currently at Newcastle University, School of Mechanical and Systems Engineering,
Newcastle upon Tyne, NE1 7RU, UK

Abstract

Carbonation of hydrous minerals and of calcium hydroxide ($\text{Ca}(\text{OH})_2$) in particular, is an important process in environmental and industrial applications for the construction industry, geological disposal repositories for nuclear waste and green technologies for carbon capture. Although the role of ions during the carbonation mechanism of $\text{Ca}(\text{OH})_2$ is still unclear, we identified the exchange of ions during the dissolution-and-precipitation process, by determining the change in isotopic composition of carbonation products using Time-of-Flight Secondary Ion Mass Spectrometry. Our samples of pure $\text{Ca}(^{18}\text{OH})_2$ carbonated in air were characterized using Scanning Electron Microscopy and Raman spectroscopy, aided by Density Functional Theory calculations.

Our results show that the carbonation process at high pH is a two-stage mechanism. The first stage occurs in a short time after $\text{Ca}(^{18}\text{OH})_2$ is exposed to air and involved the dissolution of surface Ca ions and hydroxyl ^{18}OH groups, which reacts directly with dissolved CO_2 , leading to 1/3 of ^{18}O in the oxygen content of carbonate phases. The second stage occurs within 24h of exposure allowing a rebalance of the oxygen isotopic composition of the carbonate phases with higher content of ^{16}O .

Introduction

The carbonation process of hydrous materials and minerals such as calcium and magnesium hydroxides ($\text{Ca}(\text{OH})_2$ and $\text{Mg}(\text{OH})_2$, respectively) is important for a number of environmental and technological applications. These include carbon capture and storage (CCS)^{1,2}, scrubbing procedures of solid waste incinerators³, emerging low carbon building technologies for construction⁴⁻⁶, and geological disposal repositories for nuclear waste^{7,8} where portlandite content in cements becomes a critical factor. Despite its importance,^{2,4,9-14} the carbonation mechanism in high pH environment is debated and not yet fully understood. Hence, to devise

successful and efficient strategies for carbon dioxide (CO₂) sequestration, soil stabilization in geoen지니어ing and building mortars with enhanced properties, a clear understanding of the details of carbonation mechanisms is required.

Two carbonation mechanisms have been proposed for portlandite at low temperature and pressure (i.e. STP). These are based on a solid state and a dissolution-carbonation¹⁵⁻¹⁹ process (the former is highly unlikely whereas the latter has been documented in a number of cases). Moorehead²⁰ suggested that carbonation of Ca(OH)₂ at room temperature in CO₂-rich environments is a solid-state reaction, which entails substitution of hydroxyl groups (OH⁻) with carbonate groups (CO₃²⁻) in a topotactic transition, leading to a change of the portlandite $d_{\{001\}}$ spacing.^{11,20-22} Other authors suggested that the reaction occurs via a dissolution-and-precipitation mechanism catalyzed by water molecules adsorbed on the mineral surfaces^{11,23,26} (a detailed description of the carbonation mechanisms has been recently published by Rodriguez Navarro and colleagues²⁶⁻²⁷). Overall, these two mechanisms would be expected to lead to different reaction rates, and to the formation of passivating carbonate layers²⁵ that quenches the exploitation of Ca(OH)₂ surface properties.¹¹

The natural variation of stable isotopes, such as carbon-13 (¹³C) or oxygen-18 (¹⁸O), can be exploited in the study of carbonation of surfaces, and thus provides complementary results to other techniques.²⁹⁻³² An isotope can be traced during chemical reactions and, as different reaction mechanisms lead to different products with distinctive isotopic compositions²⁹⁻³⁴, it provides insights on the stages occurring during the reaction. Our research investigated the role of OH⁻ ions in the carbonation mechanism of Ca(OH)₂ by using Time-of-Flight Secondary Ion Mass Spectrometry (ToF-SIMS) on a Ca(¹⁸OH)₂ sample carbonated in air (rich in ¹⁶O) for 3 minutes, 1, 8 and 137 days at 27% RH (3 minutes) and 50% RH (1, 8 and 137 days).²⁶ Samples were characterized using Scanning Electron Microscopy (SEM) and Raman spectroscopy. Density functional theory calculations were also employed to corroborate the Raman shifts

associated with different degrees of isotopic substitution in $\text{Ca}(\text{OH})_2$ and CaCO_3 . We finally discuss critical factors in the carbonation process, which provides new insights of the carbonation mechanism of $\text{Ca}(\text{OH})_2$.

Experimental and Theoretical Methods

Material preparation

^{18}O -calcium hydroxide was produced by reacting calcium metal of 99% purity with isotopic labelled water containing $>99\%$ ^{18}O (Taiyo Nippon Sanso Corporation), on a platinum (Pt) foil 99.9% pure. To prevent oxygen contamination and carbonation of the $\text{Ca}(\text{OH})_2$ sample, the reaction was performed in an inert atmosphere inside a glove bag filled with nitrogen, where CO_2 and RH were monitored using a K-30 10,000ppm sensor for CO_2 , and a DHT22 sensor for temperature and humidity. Both sensors were controlled via an Arduino Uno microcontroller, which was also used for real time monitoring of the conditions.

Experiments were conducted as follows. 1) The equipment and materials were placed into a glove bag that was then filled with nitrogen. 2) The residual air in the bag was flushed using dry Nitrogen until the sensor readings were 0 ppm CO_2 and $<5\%$ RH. 3) 20mg of Ca metal was weighed on a precision balance and deposited on a Pt foil, positioned inside an open crucible. 4) 800 μl of ^{18}O -water was reacted with the Ca metal using a glass Hamilton syringe equipped with a metal needle. The reaction was carried out in an excess of ^{18}O -water to promote the complete reaction of Ca. 5). To ensure the complete evaporation of excess of ^{18}O -water, the bag was flushed several times with dry nitrogen. 6) When the majority of the water had evaporated, portions of the sample were removed from the Pt foil. Portions were sealed inside a glass cell with a quartz window for the Raman analysis; the N_2 -rich atmosphere prevented carbonation before completion of the analysis. The same procedure was followed for samples for SEM analysis except samples were placed in a small vial and stored under low vacuum.

Material for SIMS analysis was kept on Pt foil and stored in a specifically designed glass vial under low vacuum.

ToF-SIMS analysis

In order to study the isotopic composition of carbonates at the very beginning of the reaction, the first ToF-SIMS analysis was carried out after approximately 3 minutes exposure to air at $23\pm 2^\circ\text{C}$ and $27\pm 10\%$ RH. Low RH levels were used to minimize the carbonation rate.²⁶ After initial analysis, the samples were removed from the instrument and allowed to stand in a dust-free controlled environment at $23\pm 2^\circ\text{C}$ and $50\pm 10\%$ RH for 1, 8 and 138 days before further analysis. Care was taken to analyze fresh areas of the samples that had not previously been exposed to the ion and electron beams. An Analar CaCO_3 powder was analyzed under similar conditions as a reference.

Static ToF-SIMS analyses were carried out using an ION-TOF ‘TOF-SIMS IV – 200’ instrument (ION-TOF GmbH, Münster, Germany) of single-stage reflectron design.³² Positive and negative ion spectra of the samples were obtained using a Bi^{32+} focused liquid metal ion gun at 20keV energy, incident at 45° to the surface normal and operated in ‘bunched’ mode for high mass resolution. This mode used 7ns duration ion pulses at 10kHz repetition rate. Charge compensation was effected by low-energy (ca. 20eV) electrons provided by a flood gun. The total ion dose density was less than 5×10^{16} ions m^{-2} in all cases. The topography of the sample surface and the ion gun mode of operation limited the mass resolution in this work to *ca. $m/\Delta m = 4000$* .

Positive and negative ion static SIMS spectra of the samples were recorded in triplicate at room temperature with a 128×128 pixel raster and a field of view of $50\mu\text{m} \times 50\mu\text{m}$. Sample preparation and data analysis was carried out according to the procedure detailed in the SI.

Raman analysis

Raman analysis was performed using a Renishaw inVia Raman Microscope equipped with lasers operating at wavelengths of 785 nm. The analysis was undertaken by focusing the laser with a 50x long distance objective. Laser power was set to 66mW (sample) and the acquisition time was set between 3 and 10s for each of the 10 accumulations acquired. Each spectrum was taken over the wavenumber range $77\text{--}1290\text{cm}^{-1}$. Three spectra per sample were acquired to evaluate differences among the different locations. Prior to the analysis, the spectrometer was calibrated using a monocrystalline silicon standard specimen. Renishaw WiRe 4.0 software was applied for peak fitting and deconvolution of Raman spectra. The sample was initially kept in a N₂-rich atmosphere inside the glass cell with quartz window to prevent contamination by atmospheric CO₂. To investigate the initial stage of carbonation, the quartz window was removed and spectral acquisition of the carbonate phases formed at 23°C and 30%±10%RH was started. These conditions were chosen in order to reduce the carbonation rate and, therefore, have a better evidence of the phase transformations related to carbonation. Spectra were take up to 55 minutes from initial exposure of sample to air.

SEM analysis

SEM images were obtained using a JEOL field emission scanning electron microscope (FESEM) model JSM6301F. Working distance for scanning and acquiring the images was 7mm, accelerating voltage was of 5kV and the spot size 7nm. Prior to analysis the sample powder was fixed to a metal holder using a double-sided carbon tape and then dried for 24 hours in a vacuum chamber before application of a 10nm thick layer of chromium using a Quantum Q 150T Turbo-Pumped Sputter Coater to prevent surface charging. Once removed from the sputter coater, the sample was immediately inserted in the SEM and analyzed.

Computational procedure

Simulations were used to determine the vibrational shifts and Raman spectra for ¹⁶O and ¹⁸O-calcium hydroxide (Ca(¹⁶OH)₂, Ca(¹⁸OH)₂ respectively), as well as calcite containing different

amount of ^{18}O ($\text{CaC}^{18}\text{O}_x^{16}\text{O}_{(3-x)}$ with $x=0,1,2,3$). Calculations were performed at the DFT level using the VASP³⁶⁻³⁶ code with the PBE³⁹⁻⁴⁰ exchange-correlation functionals including the van der Waals correction optB86b-vdW^{41,42}, which improves the description of layered materials. The Brillouin zone was sampled using $4 \times 4 \times 4$ Monkhorst-Pack k-point mesh for portlandite and $4 \times 4 \times 1$ for calcite with a plane wave cut-off of 500 eV. Convergence criteria were 10^{-8} eV for the electronic relaxation and 10^{-4} eV \AA^{-1} for ionic forces, allowing both atoms and lattice to relax.

The calculated structure of portlandite contains 1 $\text{Ca}(\text{OH})_2$ unit and has lattice parameters of $a = b = 3.573\text{\AA}$, $c = 4.794\text{\AA}$, $\alpha = \beta = 90^\circ$ and $\gamma = 120^\circ$, which compare well with the experimental values of Desgranges et al.⁴⁴ The calculated structure of calcite contains 6 CaCO_3 units and has lattice parameters of $a = b = 5.03\text{\AA}$, $c = 16.80\text{\AA}$, $\alpha = \beta = 90^\circ$ and $\gamma = 120^\circ$, and agrees well with the experimental values of Effenberger et al.⁴⁵

From the minimized structures, the vibrational frequencies were obtained using finite displacements⁴⁶ and the Raman activity^{47,48} was then estimated by calculating the polarizability of the vibrational modes. As noted, the minimized structure for portlandite compares well with the experimental values (Table S1) and this model has recently been shown to perform well for the calcium oxide and carbonate.^{49,50} Additional calculations were undertaken to predict the shift in Raman frequencies due to isotopic substitution and compared to the DFT predicted Raman active peaks. Each vibrational mode implies certain modes that involves species. The interaction between species can be related to a bond and the strength of each bond can be illustrated considering a diatomic molecule, by a force constant k from which the frequency, f , can be calculated according to Equation 1, where μ is the reduced mass of the components of the mode given by Equation 2, where m_1 and m_2 are the masses vibrating.

$$f = \sqrt{\frac{k}{\mu}} \quad (1)$$

$$\mu = \frac{m_1 m_2}{m_1 + m_2} \quad (2)$$

When accounting for the difference in mass between ^{16}O and ^{18}O the reduced mass changes according to the O isotope. In practice, we evaluate and diagonalise the complete mass-weighted force constant matrix.⁵¹⁻⁵³

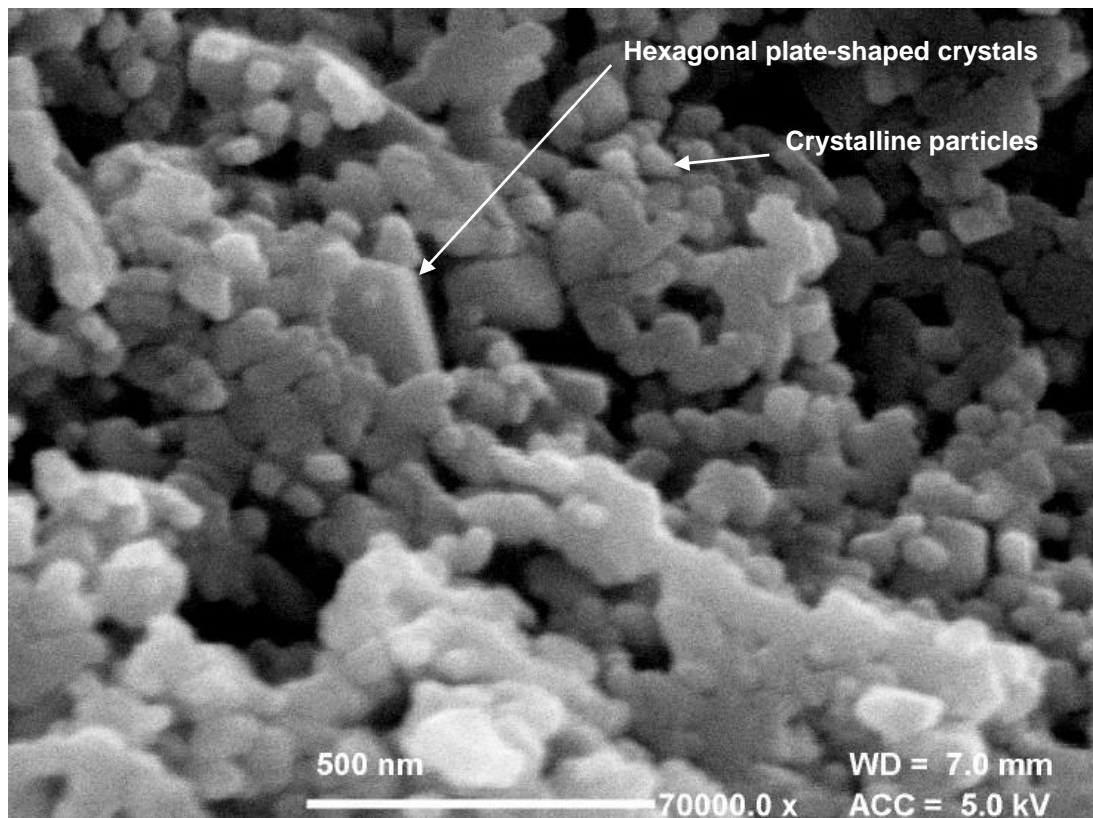


Figure 1 - FESEM image of the $\text{Ca}(^{18}\text{OH})_2$ produced

Results

SEM and Raman results

Microscopic FESEM image in Figure 1 shows $\text{Ca}(^{18}\text{OH})_2$ sample comprising of hexagonal plate-shaped crystals of 200-400nm and crystalline particles of 70-150 nm . The presence of various shaped crystals suggests a very high nucleation rate that led to numerous crystal seeds competing for growing. No crystals with the characteristic morphology of calcite or other CaCO_3 polymorph were found in the sample, and this suggests that the reaction with atmospheric CO_2 was limited during sample preparation.

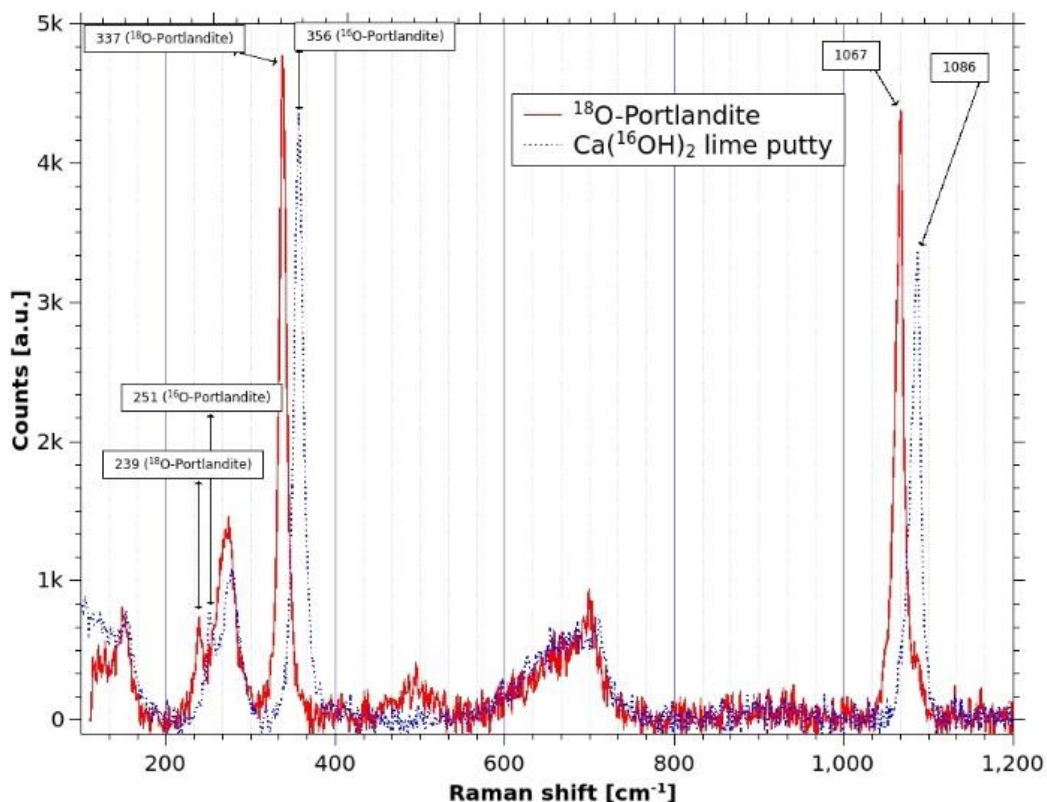


Figure 2 - Raman spectrum of the $\text{Ca}^{18}\text{OH}_2$ produced during the experiments, compared with the Raman spectrum of a generic $^{16}\text{O}\text{-Ca}(\text{OH})_2$ (lime putty).

Figure 2 shows the Raman spectrum from 100 to 1200 cm^{-1} of $\text{Ca}^{18}\text{OH}_2$ after about 10 minutes from exposure to air, compared with the spectrum of a generic ^{16}O -lime putty partially exposed to air. Both spectra contain portlandite and calcite peaks. Several peaks of $\text{Ca}^{18}\text{OH}_2$ are shifted to lower wavenumbers compared to the $\text{Ca}^{16}\text{OH}_2$: the peak at 356cm^{-1} is shifted $\sim 19\text{cm}^{-1}$ to 337cm^{-1} , the peak at 251cm^{-1} is shifted $\sim 12\text{cm}^{-1}$ to 239cm^{-1} and the peak at 1086 is shifted to 1067cm^{-1} .

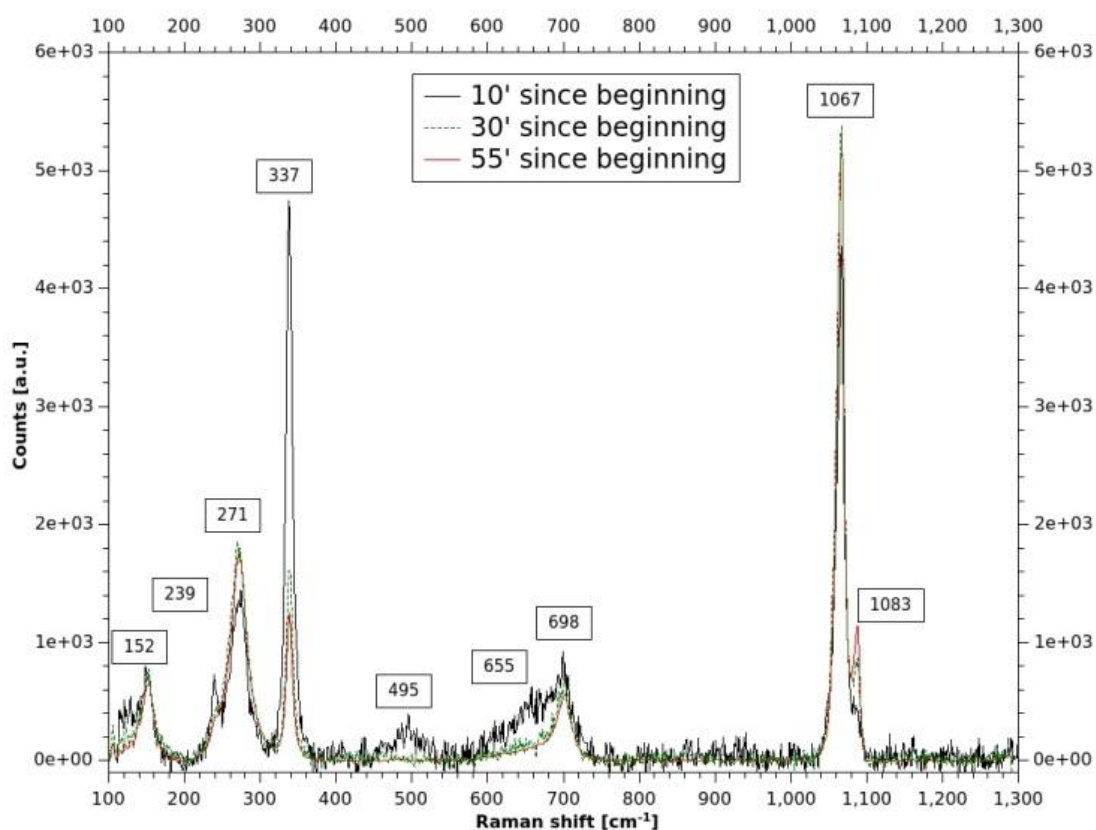


Figure 3 - Raman spectrum of the $\text{Ca}(^{18}\text{OH})_2$ produced partially carbonated. Spectra taken after 10', 30' 55' since the beginning of the tests, which exposes the sample to air.

Figure 3 shows the Raman spectra from 100 to 1300 cm^{-1} of the $\text{Ca}(^{18}\text{OH})_2$ produced, after 10, 30 and 55 minutes from the opening of the cell, which allow the sample to be in contact with air. Peaks at 239, 337 and 655 cm^{-1} are related to $\text{Ca}(^{18}\text{OH})_2$ and become weaker over the time. This provides evidence of $\text{Ca}(^{18}\text{OH})_2$ reacting with atmospheric CO_2 containing ^{16}O and forming CaCO_3 . According to our simulations, peaks at 152, 271, 698 and 1067 cm^{-1} can be associated to ^{18}O -calcite (although it is likely that the peak at 1067 cm^{-1} also includes a contribution of ^{18}O -enriched ACC; see later in this paragraph). These peaks are shifted to lower wavenumbers compared to literature spectra of ^{16}O -calcite (Table S4). Intensity of the peak at 152 cm^{-1} remains unaltered over time, whereas intensity of the peaks at 271, 698 and 1083 cm^{-1} increase, suggesting progression of the carbonation reaction with the formation of an increasing amount of ^{16}O -calcite. The broad peaks at 450 disappearing after 10 minutes

reaction, suggests presence of a metastable phase such as ACC (main peak included in the 1067cm⁻¹ peak as previously mentioned).

Computation Results

Table 1 compares Raman active modes of a natural (Ca(¹⁶OH)₂) and an isotopically labelled (Ca(¹⁸OH)₂) portlandite calculated using DFT with experimental values. Although, the relative positions of the peaks are captured for both minerals, there is a systematic displacement of the predicted peaks relative to the experimental positions⁵³. This is a well-known effect of DFT calculations and relates to the estimation of bond strengths.

Table 1 - Comparison of experimental and simulated Raman active modes of portlandite. The Raman shift due to the different O isotopes is Δ , which is compared to the theoretically derived values (Equation 1).

Experiment [cm ⁻¹]			Simulation [cm ⁻¹]			Theory [cm ⁻¹]
Ca(¹⁶ OH) ₂	Ca(¹⁸ OH) ₂	Δ	Ca(¹⁶ OH) ₂	Ca(¹⁸ OH) ₂	Δ	Δ
251	239	-12	256	242	-14	-14
356	337	-19	381	361	-20	-19
675	675	0	715	715	0	0

The two low frequency peaks of portlandite are associated with vibrations of the hydroxide ions relative to each other in plane and out of plane. In the case where two hydroxide ions are vibrating as whole units the individual masses in the pure case are $m_1=m_2=17$ while for full isotopic substitution with ¹⁸O these increase to $m_1=m_2=19$. The reduced masses are 17/2 and 19/2 respectively, and thus the theoretical treatment as in Equation 1 predicts the isotopically doped system has a frequency to $(17/19)^{1/2}$ of the natural case corresponding to shifts of -14cm⁻¹ (for peak 1 at 251cm⁻¹) and -19cm⁻¹ (peak 2). In contrast, the high frequency portlandite peak

at 675cm^{-1} is associated with the rocking mode of individual hydroxide ions. Since this is a rotational vibration, any shift is due not to the change in effective mass associated with isotopic substitution but with the moment of inertia. The resulting Raman shift due to isotopic composition is predicted to be $\sim 0.3\%$ (compared with $\sim 5\%$ in the previous cases) which is consistent with no observed shift in the experimental and simulated spectra. Comparison of calculated and experimental peak positions provides evidence that Raman spectroscopy can distinguish between different isotope compositions of the same material as already suggested by Ruiz-Agudo et al.⁵⁴

Calcite with different isotopic composition ($\text{CaC}^{16}\text{O}_x^{18}\text{O}_{3-x}$) shows Raman shifts at higher wave number with increasing x , the number of ^{18}O per carbonate ion (Table 2). The peak at about 152 cm^{-1} in the experimental spectra is noisy and difficult to isolate in both natural and ^{18}O -sample but the remaining Raman active peaks are relatively well defined and more easily characterized. Overall, the computational results are in good agreement with the measured spectra. The advantage of the calculation is that the vibrational motion associated with each active mode can be identified.⁵² For example, we can clearly identify the high frequency peak as the symmetric stretch of the C-O bond in the carbonate ions, whereas the peak at 700 cm^{-1} is an antisymmetric coupling between carbonate ions in different layers. The vibrations of the remaining peaks are complex motions of carbonate bending in different layers.

Table 2 - Comparison of experimental and simulated Raman active modes of calcite. In brackets the Raman shift due to the different O isotopes compared to $\text{CaC}^{16}\text{O}_3$. The two columns in the experimental results are related to carbonate phases with different ^{18}O content.

Peak	Experiment [cm^{-1}]		Simulation [cm^{-1}]			
	CaCO_3	CaCO_3	$\text{CaC}^{16}\text{O}_3$	$\text{CaC}^{18}\text{O}^{16}\text{O}_2$	$\text{CaC}^{18}\text{O}_2^{16}\text{O}$	$\text{CaC}^{18}\text{O}_3$

	$\frac{^{18}\text{O}}{^{16}\text{O}} >$	$\frac{^{18}\text{O}}{^{16}\text{O}} <$				
1	152	152	159-165	156-162 (-3)	154-160 (-5)	151-157 (-8)
2	277	282	293	288 (-5)	285 (-8)	282 (-11)
3	698	713	680	672-665 (-8/-15)	661-652 (-19/-28)	645 (-35)
4	1066	1086	1055	1036 (-19)	1015 (-40)	995 (-60)

ToF-SIMS Results

ToF-SIMS allows the determination of the elemental, isotopic, or molecular composition of surfaces to a maximum depth of 1-2 nm. It is a destructive technique that reveals, using a mass spectrometer, the mass:charge ratio of secondary ions ejected from the surface when a primary ion beam is fired against it. Therefore, during the analysis secondary ions may be positively and negatively charged depending on their composition and mass. Data analysis has therefore to take into account both polarities. Full details of mass:charge ratio of ejected secondary ions considered in this study are in Table S2 and Table S3 where a detailed analysis of the results is also reported. To assess the accuracy of the ToF-SIMS measurement, we tested an Analar CaCO_3 reference sample, which gave an average $^{18}\text{O}:^{16}\text{O}$ ratio of 0.021 (Table 3) in agreement with the isotopic ratio between 0.019 and 0.021⁵⁷⁻⁵⁹ of naturally occurring samples. Data for the carbonated $\text{Ca}(^{18}\text{OH})_2$ samples, show a reduction in the relative intensities of species containing ^{18}O over the time, and a simultaneous increase of the intensities of species containing ^{16}O (Figures S1-S3 in the SI). Simultaneously, species containing carbon such as $[\text{HC}^{18}\text{O}_3]^-$ and $[\text{C}^{18}\text{O}_3]^-$ (Figures S1-S3) show an increase. This is clear evidence of the carbonation of portlandite surfaces as secondary ions ejected from the surface destruction have greater carbon content.

Table 3 reports the $^{18}\text{O}:^{16}\text{O}$ ratio calculated for all the secondary ions produced by the destruction of the surface over the duration of the experiment. Data shows an initial isotope ratio of 0.62 for positive ions and a ratio of 0.51 for negative ions. The weighted average value

of 0.54 suggests that, at very early stage of the carbonation reaction, for every atom of ^{18}O in carbonate ions, there would be two ^{16}O (theoretical $^{18}\text{O}:^{16}\text{O}$ ratio 0.5). However, from day 0 to day 1 the data shows a dramatic decrease in the $^{18}\text{O}:^{16}\text{O}$ ratio to a value of 0.038 that shows little variation in the following days. This value shows little variation after 137 days of carbonation. The isotope ratio for positive and negative species converges towards the same value of 0.046, which is approximately double the value for natural samples.

Table 3 - $^{18}\text{O}:^{16}\text{O}$ ratio calculated from the intensity of the ToF-SIMS counts for the ionic species with positive and negative polarity

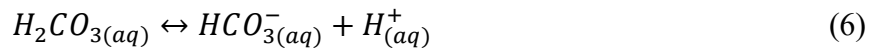
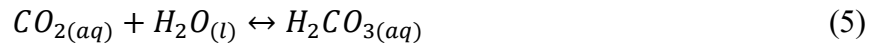
	Analar CaCO_3	Carbonated $\text{Ca}(^{18}\text{OH})_2$			
		Day 0	Day 1	Day 8	Day 137
$[^{18}\text{O}/^{16}\text{O}]^+$	0.035	0.616	0.057	0.044	0.046
$[^{18}\text{O}/^{16}\text{O}]^-$	0.007	0.509	0.032	0.029	0.046
Weighted Average	0.014	0.537	0.038	0.033	0.046

Discussion

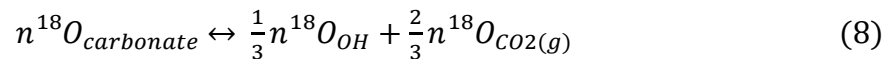
The combination of complementary results from the vibrational fingerprint of the materials with different isotopic composition and the ToF-SIMS experiments show that we can elucidate the carbonation mechanism of hydrous materials. However, before discussing our data, the role of the pH in the carbonate precipitation and on the behavior of different isotopes during the process should be highlighted.

Recent work on the precipitation of carbonates in natural systems (i.e. at approximately neutral pH) shows that an isotopic equilibrium is reached between the solution and the precipitated solid, which only depends on temperature.^{34,59} On the other hand, precipitation of carbonates from saturated solutions of $\text{Ca}(\text{OH})_2$ takes place under high pH (12.4 at 23°C)¹⁴ and

therefore is in non-equilibrium conditions. As a consequence, the main phenomenon producing fractionation during precipitation is the reaction kinetics related to the solution high pH.²⁹⁻³³ At pH above 9, various authors^{29,31-33} suggested that the direct reaction of CO₂ with the hydroxyl group (OH⁻) produced by the dissociation of water is the primary pathway for carbonate ion formation (Equation 3).²⁹ This pathway is suggested to be faster than the one leading to the formation of CO₃²⁻ from the reaction of CO₂ in natural waters at neutral pH⁵⁸ (Equations 4-7) and, consequently, it prevents isotope equilibration of gaseous CO_{2(g)} with the dissolved CO_{2(aq)} (Equation 4). Since heavier isotopes react slower than lighter isotopes, in the carbonate precipitates at high pH we would expect a lower concentration of ¹⁸O and ¹³C compared to the carbonates precipitated under equilibrium conditions.²⁹ Examples of carbonate phases with a very different isotope signature are limestone of marine and continental origins, and carbonates produced during cement setting.³¹⁻³³



Equilibrium in Equation 3 implies that the carbonate ion contains a mixture of the isotopic composition of aqueous CO_{2(aq)} (similar to the isotopic composition of gaseous CO_{2(g)}) and OH⁻ ions.^{29,31,33} The ¹⁸O composition of these carbonates (*n¹⁸O*) can be described by considering the abundance of ¹⁸O in the different species, according to Equation 8.



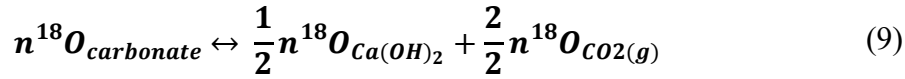
Letolle et al.²⁹ have calculated that one third of the oxygen in the carbonates formed under conditions of high pH, is provided by the OH⁻ ions originated from the dissociation of H₂O molecules catalyzing the reaction between Ca(OH)₂ and aqueous CO_{2(aq)}. This implies that ¹⁸O content of OH⁻ groups is related to the isotopic composition of H₂O. Letolle et al.²⁹, however, did not provide any information on the role of OH⁻ ions produced by the dissolution of Ca(OH)₂ on the isotopic composition of carbonate phases.

To demonstrate that hydroxyl groups from the surface have a fundamental role in the formation of carbonate phases, we have studied Ca(¹⁸OH)₂ samples made of ¹⁸O. Therefore, during the carbonation of Ca(¹⁸OH)₂, the sample itself is by far the most important source of ¹⁸O (a very limited contribution can be due to the CO₂ and H₂O^{60,61}) whereas the atmospheric water and CO₂ are the only source of ¹⁶O. Any mixture of the isotope in the resulting carbonate phases provides the most likely source of oxygen in the formation of carbonate ions and therefore the carbonation mechanism.

The Raman spectrum of Ca(¹⁸OH)₂ confirms the purity of the sample but also the high surface reactivity, as demonstrated by the formation of carbonate phases after 10 minutes from exposure to atmospheric CO₂. This is in agreement with the results of previous studies on the carbonation kinetics and on the role of water vapor on the Ca(OH)₂/CO₂ solid-gas reaction.^{12,62} The shift observed for the Raman peaks of portlandite and calcite can be associated with variations in the isotopic composition of the minerals and are supported by ab initio calculations. In the case of portlandite, the shifts in the Raman peaks arise from substitution of all the ¹⁶O with ¹⁸O (Figure 2), whereas the shift in the Raman peaks of carbonate phases formed after the reaction with atmospheric CO₂ arise from partial substitution of ¹⁶O with ¹⁸O (Figure 3). DFT data (Table 2) support that the experimental peaks at 152, 271, 698 and 1066 cm⁻¹ are associated with calcite containing 1/3 of ¹⁸O (¹⁸O:¹⁶O ratio 0.5). The main vibrational fingerprint of this phase could be identified in the peak at 1066 cm⁻¹ (Figure 3). The peak at

1083 cm^{-1} belongs to ^{16}O -calcite, which is a minor phase at the beginning of the reaction but that grows over the time.

SIMS results allow calculation of the $^{18}\text{O}:^{16}\text{O}$ ratio for the secondary ions ejected from surface destruction. At the early stage of carbonation (~3 minutes exposure to air), the ratio is of 0.51 (Table 3). This value is in good agreement with the results of our theoretical analysis of Raman shifts and with Letolle's proposition²⁹ indicating that in carbonate precipitates at high pH, 2/3 of oxygen is supplied by CO_2 whereas 1/3 of the oxygen is provided by OH^- ions. However, unlike Letolle's proposition suggesting that the OH^- groups involved in the carbonation originate from the dissociation of H_2O molecules, our results clearly demonstrate that the $\text{Ca}(\text{OH})_2$ plays an important role in the formation of hydroxyl groups. ToF-SIMS data displays carbonate species that contain 1/3 of ^{18}O (the remaining 2/3 comes from C^{16}O_2), which in our case can only be produced by the dissolution of the surface and not by the dissociation of adsorbed water molecules, which comprise mainly ^{16}O . This is also supported by PHREEQC^{57,63} modelling (see model description and Table S5 in the SI) showing that concentration of OH^- ions produced by the dissolution of $\text{Ca}(\text{OH})_2$ in pure water at 25°C, is several orders magnitude greater than the concentration of OH^- ions produced by the natural dissociation of pure water. Therefore, the OH^- ions from $\text{Ca}(\text{OH})_2$ are more likely to take part in carbonation reaction than those from water. As a consequence, it is possible to infer that in highly alkaline conditions, the isotopic composition of precipitated carbonates, which is generally described by Equation 8, can be rewritten by considering the abundance of ^{18}O in the CO_2 and in the $\text{Ca}(\text{OH})_2$ as reported in Equation 9. This new equation marks the very early part of the first stage of the carbonation reaction where the dissolution of the surface is the rate limiting step. Although this equation can be an oversimplification of the real process (since it is unknown what fraction of the resulting carbonates forms via this pathway), it can be used as a simple description of the process.



Subsequent to the formation of ^{18}O rich carbonate phases in the first stage of the carbonation mechanisms, where the dissolution of portlandite surfaces must occur, our ToF-SIMS data show a dramatic reduction in $^{18}\text{O}:^{16}\text{O}$ ratio within the first day of carbonation (Table S6). This is also shown by the growth of the Raman peak at 1083 cm^{-1} of ^{16}O -calcite over time (Figure 3) and can be explained by the transformation of the initial metastable carbonates into more stable phases over time.⁶⁴⁻⁷⁷ Figure 3 shows also disappearance over the time of a peak at 495 cm^{-1} that can be related to metastable hydrated phases⁵⁵. A possible explanation of this re-equilibration of $^{18}\text{O}:^{16}\text{O}$ ratio is the dissolution of metastable phases that give in some ^{18}O and the subsequent recrystallization of more stable phases that acquire some ^{16}O during the precipitation process happening in equilibrium conditions.

This marks the second stage of the carbonation, which involves the transformation of less to more stable carbonate phases. A detailed explanation of this transformation has been recently provided by Rodriguez Navarro et al.²⁷

Earlier, Rodriguez-Blanco et al.⁷⁰ described the transformation mechanism of ACC to calcite as a two stage process: 1) ACC particles rapidly dehydrate and crystallize forming individual particles of vaterite; 2) the vaterite dissolves and re-precipitates as calcite (Ogino et al.⁷¹ also confirmed the latter stage also for aragonite). Stage 1, mainly entails the release of water molecules initially embedded in the structure of hydrated phases. Stage 2, involves the release of CO_3^{2-} ions that, according to equations 2-5, can lead to an exchange of oxygen atoms with the water molecules. We infer that our data is consistent with this proposition. The oxygen exchange and the formation of new carbonate phases richer in ^{16}O at the top of the carbonate phases initially formed (stage 1) explains the sudden variation of the $^{18}\text{O}:^{16}\text{O}$ ratio within the first 24h. Therefore, it is possible to infer that, whereas precipitation of meta-stable phases

takes place in non-equilibrium conditions (i.e. at high pH, which does not allow isotope equilibration), the dissolution-and-precipitation mechanism leading to the formation of stable carbonate phases and the precipitation of new carbonate phases richer in ^{16}O , occurs at lower pH allowing an isotopic equilibrium of carbonates. It is worth noting that in our experiments this equilibration occurred within the initial 24 hours even at 50% RH (a relatively low RH value for carbonation) and this suggests that stage 2 of the carbonation is a fast kinetic pathway.

Conclusions

Our results show new insights in the carbonation mechanism of portlandite. They demonstrate that during the early stage of the carbonation reaction (first 3 minutes, in our experiments) the surface hydroxyl groups are the source of oxygen for the formation of carbonate ions and hence the growth of carbonate begins by the dissolution of hydroxyl and Calcium ions followed by the formation of metastable calcium carbonate. The second stage of the reaction occurs within the 24h after the carbonation started. This involves the transformation of the metastable carbonate phases into stable calcite. During this transformation there is a release of water, which is the source of oxygen for the formation of new carbonate ions.

This is extremely valuable in understanding the evolution of Portland cements for usage in construction industry and in geological disposal facilities for nuclear waste as well as in devise of successful green technologies for carbon sequestration and storage because it introduces a new paradigm in the formation of carbonate ion during precipitation of carbonates.

Acknowledgements

The authors would like to thank the Engineering and Physical Sciences Research Council (EPSRC) for financial support through project EP/K025597/1. The computational work has made use of ARCHER, the UK's national HPC, via the Materials Chemistry Consortium funded by the EPSRC (EP/L000202) in addition to the University of Bath's HPC resource. The

authors are grateful to Mrs Ursula Potter and Dr Philip Fletcher of the Microscope and Analysis Suite of the University of Bath for assistance with SEM imaging and Raman spectroscopy. All data supporting this study are openly available from the University of Bath data archive at 10.15125/BATH-00240.

Supporting Information Description

(1) ToF-SIMS sample preparation; (2) ToF-SIMS data analysis; (3) PHREEQC calculations; (4) detailed plots of the SIMS results; (4) experimental and simulated lattice parameters for portlandite; (5) Plot of the $^{18}\text{O}:^{16}\text{O}$ ratio over the time; (6) Table of experimental and simulated lattice parameters for portlandite; (7) List of all ions considered in this research; (8) list of ions considered for calculating the $^{18}\text{O}:^{16}\text{O}$ ratio; (9) peak position of the Raman spectra for different CaCO_3 phases; (10) OH^- concentration in different aqueous solutions, calculated using PHREEQC. This information is available free of charge via the Internet at <http://pubs.acs.org>.

References

- 1) Blamey, J.; Lu, D. Y.; Fennell, P. S.; Anthony, E. J. Reactivation of CaO-based sorbents for CO_2 capture: mechanism for the carbonation of $\text{Ca}(\text{OH})_2$, *Industrial & Engineering Chemistry Research*. **2011**, 50 (17), 10329-10334.
- 2) Zhao, L.; Sang, L.; Chen, J.; Ji, J.; Teng, H. H. Aqueous carbonation of natural brucite: relevance to CO_2 sequestration, *Environmental Science & Technology* **2010**, 44 (1), 406-411
- 3) Sawell, S.E.; Chandler, A.J.; Eighmy, T.T.; Hartlan, J.; Hjelmar, O.; Kosson, D.; van der Sloot, H.A.; Vehlow, J. The international ash working group: A treatise on residues from {MSW} incinerators, In *Environmental Aspects of Construction with Waste Materials*; van der Sloot, H.A.; Goumans, J.J.J.M.; Aalbers, Th.G. Eds. Proceeding of the International Conference on Environmental Implications of

Construction Materials and Technology Developments volume 60 of Studies in Environmental Science; Elsevier: **1994**; pp 3-6.

- 4) Gartner, E.; Hirao, H. A review of alternative approaches to the reduction of CO₂ emissions associated with the manufacture of the binder phase in concrete. *Cement and Concrete Research*. **2015**, 78 Part A, 126-142.
- 5) Pesce, G.L.; Bowen, C. R.; Rocha, J.; Sardo, M.; Allen, G.; Walker, P.; Denuault, G.; Serrapede, M.; Ball, R. J. Monitoring hydration in lime-metakaolin composites using electrochemical impedance spectroscopy and nuclear magnetic resonance spectroscopy. *Clay Minerals*. **2014**, 49, 341-358.
- 6) Berger, R. Calcium Hydroxide: Its Role in the Fracture of Tricalcium Silicate Paste. *Science*, **1972**, 175(4022), 626-629
- 7) Corkhill, C.L.; Bridge, J.W.; Chen, X.C. et al. Real-Time Gamma Imaging of Technetium Transport through Natural and Engineered Porous Materials for Radioactive Waste Disposal. *Environmental Science & Technology*. **2013**, 47(23), 13857-13864
- 8) Ewing, R.C. Long-term storage of spent nuclear fuel. *Nature Materials*. **2015**, 14(4), 252-257
- 9) Hovelmann, J.; Putnis, C. V.; Ruiz-Agudo, E.; Austrheim, H. Direct nanoscale observations of CO₂ sequestration during brucite [Mg(OH)₂] dissolution, *Environmental Science & Technology*. **2012**, 46(9), 5253-5260.
- 10) Allen, A.J.; Jeffrey, J.; Jennings, H.M. Composition and density of nanoscale calcium silicate-hydrate in cement. *Nature Materials*. **2007**, 6(4), 311-316

- 11) Ruiz-Agudo, E.; Kudlacz, K.; Putnis, C. V.; Putnis, A.; Rodriguez-Navarro, C. Dissolution and carbonation of portlandite [Ca(OH)₂] single crystals, *Environmental Science & Technology*. **2013**, 47(19), 11342-11349.
- 12) Cizer, O.; Rodriguez-Navarro, C.; Ruiz-Agudo, E.; Elsen, J.; Gemert, D.; Balen, K. Phase and morphology evolution of calcium carbonate precipitated by carbonation of hydrated lime, *Journal of Materials Science*. **2012**, 47 (16), 6151-6165.
- 13) Cizer, O.; Van Balen, K.; Elsen, J.; Van Gemert, D. Realtime investigation of reaction rate and mineral phase modifications of lime carbonation. *Construction and Building Materials*. **2012**, 35, 741-751
- 14) Serrapede, M.; Pesce, G.L.; Ball, R.J.; Denuault, G. Nanostructured Pd hydride microelectrodes: In situ monitoring of pH variations in a porous medium. *Analytical Chemistry*. **2014**, 86 (12), 5758-5765
- 15) Kitamura, M.; Konno, H.; Yasui, A.; Masuoka H. Controlling factors and mechanism of reactive crystallization of calcium carbonate polymorphs from calcium hydroxide suspensions. *Journal of Crystal Growth*. **2002**, 236 (1-3), 323–332.
- 16) Domingo, C.; Garcia-Carmona, J.; Loste, E.; Fanovich, A.; Fraile, J.; Gomez-Morales, J. Control of calcium carbonate morphology by precipitation in compressed and supercritical carbon dioxide media. *Journal of Crystal Growth*. **2004**, 271 (1-2), 268–273.
- 17) Sheng Han, Y.; Hadiko, G.; Fuji, M.; Takahashi, M. Crystallization and transformation of vaterite at controlled pH. *Journal of Crystal Growth*. **2006**, 289 (1), 269–274.

- 18) Euvrard, M.; Membrey, F.; Filiatre, C.; Foissy, A.. Crystallization of calcium carbonate at a solid/liquid interface examined by reflection of a laser beam. *Journal of Crystal Growth*. **2004**, 265 (1-2), 322–330.
- 19) Despotou, E.; Schlegel, T.; Shtiza, A.; Verhelst, F. Literature study on the rate and mechanism of carbonation of lime in mortars, In *Proceeding of the 9th International Masonry Conference*. **2014**. Guimaraes, Portugal on 7-9 July 2014.
- 20) Moorehead, D.R. Cementation by the carbonation of hydrated lime. *Cement and Concrete Research*. **1986**, 16 (5), 700-708.
- 21) Stepkowska, E.T. Hypothetical transformation of $\text{Ca}(\text{OH})_2$ into CaCO_3 in solid-state reactions of portland cement. *Journal of Thermal Analysis and Calorimetry*. **2005**, 80 (3), 727-733.
- 22) Montes-Hernandez, G.; Daval, D.; Chiriac, R.; Renard, F. Growth of nanosized calcite through gas-solid carbonation of nanosized portlandite under anisobaric conditions. *Crystal Growth & Design*. **2010**, 10 (11), 4823-4830.
- 23) Yang, T.; Keller, B.; Magyari, E.; Hametner, K.; Gunther, D. Direct observation of the carbonation process on the surface of calcium hydroxide crystals in hardened cement paste using an atomic force microscope, *Journal of Materials Science*. **2003**, 38 (9), 1909-1916.
- 24) Johnstone J. R.; Glasser, F. P. Carbonation of portlandite single crystals and portlandite in cement paste, In *9th International Congress on the Chemistry of Cement* volume 5 , **1992**, 370-376.

- 25) Rodriguez Navarro C.; Vettori I.; Ruiz-Agudo E. Kinetics and Mechanism of Calcium Hydroxide Conversion into Calcium Alkoxides: Implications in Heritage Conservation Using Nanolimes, *Langmuir*, **2016**, 32(20), 5183-5194
- 26) Rodriguez-Navarro C.; Elerta K.; Ševčík R. Amorphous and crystalline calcium carbonate phases during carbonation of nanolimes: implications in heritage conservation, *CrystEngComm*. **2016**, 18, 6594-6607
- 27) Rodriguez-Navarro, C.; Kudłacz, K.; Cizer, Ö.; Ruiz-Agudo, E. Formation of amorphous calcium carbonate and its transformation into mesostructured calcite. *CrystEngComm*, 2015, 17(1), 58-72
- 28) Galan, I.; Glasser, F.P.; Baza, D.; Andrade, C., Assessment of the protective effect of carbonation on portlandite crystals. *Cement and Concrete Research*, **2015**, 74, 68-77
- 29) Letolle, R.; Gegout, P.; Gaveau, B.; Moranville-Regourd, M. Fractionnement isotopique de l'oxygène-18 dans la précipitation des carbonates a pH très élevé. *Comptes Rendus de l'Académie des Sciences*. **1990**, 310, 547-552.
- 30) Van Strydonck, M.; Dupas, M.; Keppens, E. "Isotopic fractionation of oxygen and carbon in lime mortar under natural environment conditions. *Radiocarbon*. **1989**, 31, 610-618.
- 31) Létolle, R.; Gégout, P.; Moranville-Regourd, M.; Gaveau, B. Carbon-13 and oxygen-18 mass spectrometry as a potential tool for the study of carbonate phases in concrete. *Journal of the American Ceramic Society*. **1990**, 73, 3617-3625.
- 32) Rafai, N.; Letolle, R.; Blanc, P.; Person, A.; Gegout, P. Isotope geochemistry (^{13}C , ^{18}O) of carbonation processes in concretes. *Cement and Concrete Research*. **1991**, 21, 368-377.

- 33) Letolle, R.; Gegout, P.; Rafai, N.; Revertegat, E. Stable isotopes of carbon and oxygen for the study of carbonation/decarbonation processes in concretes. *Cement and Concrete Research*. **1992**, 22, 235-240, Special Double Issue Proceedings of Symposium D of the E-MRS Fall Meeting 1991.
- 34) Kosednar-Legenstein, B.; Dietzel, M.; Leis, A.; Stingl, K. Stable carbon and oxygen isotope investigation in historical lime mortar and plaster. Results from field and experimental study. *Applied Geochemistry*. **2008**, 23, 2425-2437.
- 35) Schwieters J.; Cramer H.G.; Heller T.; Jürgens U.; Niehuis E.; Zehnpfenning J.; Benninghoven A. High mass resolution surface imaging with a time-of-flight secondary ion mass spectroscopy scanning microprobe *J. Vac. Sci. Technol. A*. **1991**; 9, 2864.
- 36) Kresse, G.; Furthmüller, J., Efficient iterative schemes for ab initio total-energy calculations using a plane-wave basis set. *Physical Review B*, **1996**, 54(16), 11169-11186
- 37) Kresse, G.; Hafner, J., Ab initio molecular-dynamics simulation of the liquid-metal\char21amorphous-semiconductor transition in germanium. *Physical Review B*, **1994**, 49(20), 14251-14269
- 38) Kresse, G.; Hafner, J., Ab initio molecular dynamics for liquid metals. *Physical Review B*, **1993**, 47(1), 558-561
- 39) Kresse, G.; Joubert, D., From ultrasoft pseudopotentials to the projector augmented-wave method. *Physical Review B*, **1999**, 59(3), 1758-1775
- 40) Perdew, J. P.; Burke, K.; Ernzerhof, M., Generalized Gradient Approximation Made Simple. *Physical Review Letters*, **1996**, 77 (18), 3865-3868

- 41) Klimeš, J.; Bowler, D. R.; Michaelides, A., Van der Waals density functionals applied to solids. *Physical Review B*, **2011**, 83(19), 195131
- 42) Klimeš, J.; Bowler, D. R.; Michaelides, A., Chemical accuracy for the van der Waals density functional. *Journal of Physics: Condensed Matter*. **2010**, 22(2), 022201
- 43) Wu, X.; Vanderbilt, D.; Hamann, D. R., Systematic treatment of displacements, strains, and electric fields in density-functional perturbation theory. *Physical Review B*. **2005**, 72(3), 035105
- 44) Desgranges, L.; Grebille, D.; Calvarin, G.; Chevrier, G.; Floquet, N.; Niepce, J.C. Hydrogen thermal motion in calcium hydroxide: Ca(OH)₂, *Acta Crystallographica, Section B: Structural Science*. **1993**. 49, 812-817
- 45) Effenberger, K. H. M.; Zemann, J. Crystal structure refinements of Magnesite, Calcite, Rhodochrosite, Siderite, Smithonite, and Dolomite, with the discussion of some aspects of the stereochemistry of Calcite type carbonates, *Zeitschrift fuer Kristallographie*. **1981**, 156, 223-243
- 46) Fonari, A.; Stauffer, S., vasp_raman.py. <https://github.com/raman-sc/VASP/>: **2013**
- 47) Porezag, D.; Pederson, M. R., Infrared intensities and Raman-scattering activities within density-functional theory. *Physical Review B*. **1996**, 54 (11), 7830-7836
- 48) Porezag, D.; Pederson, M. R. Infrared intensities and Raman-scattering activities within density-functional theory. *Physical Review B*. **1996**, 54, 7830-7836
- 49) Andreassen, J.-P. Formation mechanism and morphology in precipitation of vaterite—nano-aggregation or crystal growth? *Journal of Crystal Growth*, **2005**, 274 (1-2), 256–264.

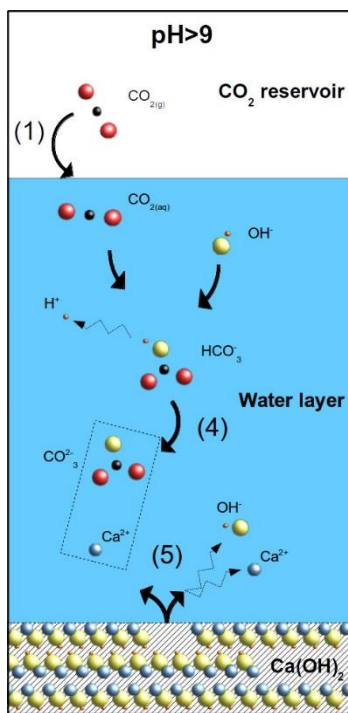
- 50) Grant, J.; Pesce, G.L.; Ball, R.J.; Molinari, M.; Parker, S.C. An Analytical and Computational Study to Resolve the Composition of Dolimitic Lime. *RCS Advances*, **2016**, 6(19), 16066-16072
- 51) Price, G.D.; Parker, S.C.; Leslie, M. The lattice-dynamics and thermodynamics of the Mg₂SiO₄ polymorphs. *Physics and Chemistry of Minerals*. **1987**, 15(2), 181-190
- 52) Cooke, D.J.; Parker, S.C.; Osguthorpe, D.J. Calculating the vibrational thermodynamic properties of bulk oxides using lattice dynamics and molecular dynamics. *Physical Review B*. **2003**, 67(13), 134306
- 53) Skelton, J.M.; Parker, S.C.; Togo, A.; Tanaka, I.; Walsh, A. Thermal physics of the lead chalcogenides PbS, PbSe, and PbTe from first principles. *Physical Review B*. **2014**, 89(20), 205203
- 54) Ruiz-Agudo E.; King H.E.; Patiño-López L.D.; Putnis C.V.; Geisler T.; Rodríguez-Navarro C.; Putnis A. Control of silicate weathering by interface-coupled dissolution-precipitation processes at the mineral-solution interface. *Geology*, 2016, 44(7), 567-570
- 55) Tlili, M. M.; Ben Amor, M.; Gabrielli, C.; Joiret, S.; Maurin, G.; & Rousseau, P. Characterization of CaCO₃ hydrates by micro-Raman spectroscopy. *J. Raman Spectrosc.* **2001**, 33, 10–16
- 56) De La Pierre, M.; Carteret, C; Maschio, L.; André, E; Orlando, R.; Dovesi, R., The Raman spectrum of CaCO₃ polymorphs calcite and aragonite: A combined experimental and computational study. **2014**. *The Journal of Chemical Physics*, 140, 164509

- 57) Appelo, C. A. J.; D., P. *Geochemistry, groundwater and pollution*; Taylor & Francis, **2005**.
- 58) Morse, J.; Mackenzie, F. *Geochemistry of sedimentary carbonate*; Developments in Sedimentology 48; Elsevier Science Publisher B.V., **1990**
- 59) Hoefs, J. *Stable Isotope Geochemistry*; Springer, **2004**
- 60) Trolier M.; White J.W.C.; Tans P.P.; Masarie K.A.; Gemery P.A. Monitoring the isotopic composition of atmospheric CO₂: Measurements from the NOAA Global Air Sampling Network. *Journal of Geophysical Research: Atmospheres*. 1996, 101(D20), 25897-25916
- 61) Lee X.; Sargent S.; Smith R.; Tanner B. In situ measurement of the water vapor 18O/16O isotope ratio for atmospheric and ecological applications. *Journal of Atmospheric and Oceanic Technology*. 2005, 22(5), 555-565)
- 62) Beruto, D.T.; Botter, R. Liquid-like H₂O adsorption layers to catalyze the Ca(OH)₂/CO₂ solid–gas reaction and to form a non-protective solid product layer at 20°C. *Journal of the European Ceramic Society*, **2000**. 20(4), 497-503
- 63) Parkhurst, D. L.; Appelo, C. A. J. Description of Input and Examples for PHREEQC version 3: A Computer Program for Speciation, Batch-Reaction, One-Dimensional Transport, And Inverse Geochemical Calculations; U.S. Geological Survey: Reston, VA, **2013**.
- 64) Demichelis, R.; Raiteri, P.; Gale, J.D.; Quigley, D.; Gebauer, D. Stable prenucleation mineral clusters are liquid-like ionic polymers. *Nature Communications*. **2011**, 2, 590

- 65) Burns, K.; Wu, T.T.; Grant, C.S. Mechanisms of Calcite Dissolution Using Environmentally Benign Polyaspartic Acid: A Rotating Disk Study. *Langmuir*. **2003**, 19(14), 5669-5679
- 66) De Leeuw, N.H.; Parker, S.C. Surface Structure and Morphology of Calcium Carbonate Polymorphs Calcite, Aragonite, and Vaterite: An Atomistic Approach. *The Journal of Physical Chemistry B*. **1998**, 102(16), 2914-2922
- 67) Kerisit S.; Parker, S.C. Free Energy of Adsorption of Water and Metal Ions on the {1014} Calcite Surface. *Journal of the American Chemical Society*. **2004**, 126(32), 10152-10161
- 68) Perdikouri, C.; Putnis, C.V.; Kasiopas, A.; Putnis, A. An Atomic Force Microscopy Study of the Growth of Calcite Surface as a Function of Calcium/Total Carbonate Concentration Ratio in Solution at Constant Supersaturation. *Crystal Growth & Design*. **2009**, 9(10), 4344-4350
- 69) Kurganskaya, I.; Lutge, A. Kinetic Monte Carlo Approach To Study Carbonate Dissolution. *The Journal of Physical Chemistry C*. **2016**, 120, 6482-6492
- 70) Rodriguez-Blanco, J. D.; Shaw, S.; Benning, L. G. The kinetics and mechanisms of amorphous calcium carbonate (ACC) crystallization to calcite, via vaterite. *Nanoscale*. **2011**, 3, 265–271.
- 71) Ogino, T.; Suzuki, T.; Sawada, K. The rate and mechanism of polymorphic transformation of calcium carbonate in water. *Journal of Crystal Growth*. **1990**, 100 (1-2), 159–167.

- 72) Clarkson, J. R.; Price, T. J.; Adams, C. J. Role of metastable phases in the spontaneous precipitation of calcium carbonate. *J. Chem. Soc., Faraday Trans.* **1992**, 88, 243–249.
- 73) Kawano, J.; Shimobayashi, N.; Kitamura, M.; Shinoda, K.; Aikawa, N. Formation process of calcium carbonate from highly supersaturated solution. *Journal of Crystal Growth.* **2002**, 237-239, Part 1 (0), 419–423.
- 74) Carmona, J. G.; Morales, J. G.; Sainz, J. F.; Loste, E.; Clemente, R.R. The mechanism of precipitation of chain-like calcite. *Journal of Crystal Growth*, **2004**, 262 (1-4), 479–489.
- 75) Nehrke, G.; Van Cappellen, P. Framboidal vaterite aggregates and their transformation into calcite: a morphological study. *Journal of Crystal Growth*, **2006**, 287 (2), 528–530.
- 76) Nebel, H.; Neumann, M.; Mayer, C.; Epple, M. On the structure of amorphous calcium carbonates. a detailed study by solid-state NMR spectroscopy. *Inorganic Chemistry*, **2008**, 47 (17), 7874–7879.
- 77) Brecevic, L.; Kralj, D. On calcium carbonates: from fundamental research to application. *Croatica Chemica Acta.* **2007**, 80 (3-4), 467–484.

For Table of Contents Use Only



SYNOPSIS: At pH above 9, the direct reaction of CO_2 with the hydroxyl group produced by the dissolution of $\text{Ca}(\text{OH})_2$ is the primary pathway for carbonate ion formation. This pathway is faster than the one leading to the formation of CO_3^{2-} from the dissolution of CO_2 in natural waters at neutral pH